Materials Science & Engineering A 909 (2024) 146817

Contents lists available at ScienceDirect

Materials Science & Engineering A

journal homepage: www.elsevier.com/locate/msea

Depth-resolved mechanical behaviour of shot peened 7050-T7451 aluminium surfaces using in-situ synchrotron X-ray diffraction

A. Madariaga [a,b,*], E. Vázquez [c], D. Foster [d], E. Jimenez-Melero [a,e,**]

[a] Department of Materials, University of Manchester, Oxford Road, Manchester, M13 9PL, UK
[b] Mondragon Unibertsitatea, Engineering Faculty, Loramendi 4, 20500, Arrasate-Mondragon, Spain
[c] Ipar-Blast SL, Parque Industrial Itziar-Deba, Parcela 4, Pabellón F2-5, 20829, Itziar, Gipuzkoa, Spain
[d] ESRF – the European Synchrotron, 71 Avenue des Martyrs, 38000, Grenoble, France
[e] School of Metallurgy and Materials, University of Birmingham, Edgbaston, Birmingham, B15 2TT, UK

ARTICLE INFO

Keywords:
Aluminium alloys
Surface phenomena
Stress/strain measurements
Micromechanics
X-ray analysis

ABSTRACT

We have assessed the elasto-plastic (sub)surface behaviour of 7050-T7451 aluminium alloy treated by shot peening using S110 steel shots of 300 μm in diameter and two different intensities, namely Almen intensity (A) of 3.4 (low-intensity) and 10.9 (high-intensity). Shot peening (SP) is a cold work process applied in the aerospace industry to enhance the fatigue tolerance of structural components after machining. The local mechanical response within the SP-induced layer was depth profiled at room temperature by performing an X-ray micro-diffraction experiment in transmission geometry at a synchrotron source, during tensile loading of the specimen to rupture. The presence of a SP-induced layer in the specimen is evidenced by compressive longitudinal lattice strains (~-540 με for low-intensity and ~-4200 με for high-intensity at 0.1 mm from the surface for the *311* reflection), parallel with respect to the applied load, i.e. perpendicular to the direction of impact of the steel shots, and also by higher values of the Full-Width-at-Half-Maximum (FWHM) of the diffraction peaks than those measured in the bulk material, due to the local plastic deformation induced by shot peening. High-intensity shot peening produced a higher surface roughness (*Sa* ~13 μm), and also two times thicker deformed surface layer (~0.4 mm), than low-intensity shot peening (*Sa* ~2 μm and ~0.2 mm thick deformed layer). For both shot peening conditions, the local yield stress of the surface layer and bulk material were similar, however the severely affected layers exhibit a non-linear elastic behaviour when applying loads lower than the yield stress of the material. Beyond yielding, the presence of SP-induced layers is mainly evidenced by the relatively higher value of the FWHM near-surface compared to the bulk (~20 % higher for low-intensity and ~40 % for high-intensity), due to the initial plastic deformation accumulated during shot peening and additional plasticity during loading of the specimen.

1. Introduction

Large thin-walled monolithic components in the aerospace industry are commonly manufactured using 7XXX aluminium alloys, due to their high specific strength and good formability [1]. The fatigue behaviour of those aerospace components after machining, depends on their surface integrity in terms of roughness, residual stresses, micro-hardness and local changes in microstructure [2,3]. Despite the machining conditions being selected to ensure a good surface quality, a final shot peening (SP) treatment is usually applied to enhance the surface integrity and fatigue tolerance of the component [4–7]. Shot peening is a cold work process that consists of impacting the workpiece surface with a controlled stream of small, hard spheres or shots at high speed [8]. The final characteristics of the SP-induced layer can be altered by selecting the type, diameter and velocity of the shots, or the intensity of exposure [5,9].

The compressive residual stresses generated by shot peening improve the fatigue performance of aluminium alloys [10–13], despite also inducing an increase in surface roughness [14–16]. Shot peening process parameters should be optimised to induce the maximum compressive residual stresses at/near the surface without introducing structural defects and excessive surface roughness. Under optimised conditions, the

* Corresponding author.
** Corresponding author.
E-mail addresses: aitor.madariaga@manchester.ac.uk (A. Madariaga), e.jimenez-melero@bham.ac.uk (E. Jimenez-Melero).

https://doi.org/10.1016/j.msea.2024.146817
Received 19 March 2024; Received in revised form 3 June 2024; Accepted 11 June 2024
Available online 13 June 2024

fatigue crack usually nucleates within or below the compressive residual stress field of the SP-induced surface layer [7], and those SP-induced compressive residual stresses reduce the crack propagation rate [10,17,18]. However, the beneficial effect of compressive residual stresses can be reduced if they relax during in-service loading. Fatigue lives higher than 5×10^5 cycles are reported to slightly reduce compressive residual stresses in alloy 7075-T651 [11], whereas compressive residual stresses induced by lower SP intensities are more stable [15]. Based on these experimental results, models of increasing complexity have been developed to account for the effect of SP-induced surface layers on the fatigue behaviour of 7XXX-series alloys. Those models include the effect of roughness, residual stresses and/or cold-work induced by shot peening on crack propagation and fatigue life [10,15,19]. Despite these efforts, existing models do not predict accurately the relaxation of residual stresses and fatigue crack propagation rate within the surface layer, probably because only the average mechanical properties of the surface were characterised and included in the models, and not the variation of the local mechanical properties within the SP-affected layer with sub-millimetre thickness.

The characterisation of the local mechanical behaviour of surface layers can be achieved by combining in-situ mechanical tests and X-ray diffraction experiments [20–24]. These experiments confirmed that the shot peening process for the selected parameters can significantly increase the local yield stress of the affected surface layer compared to the bulk in several materials: ~250 % higher in X42Cr13 and 55Si7 steels [20], ~300 % higher in S30432 austenitic steel [22], 27 % higher in Ti–6Al–4V alloy [23], and 59 % and 104 % in ferrite and austenite phases respectively in SAF2507 duplex stainless steel [24]. Unfortunately, the use of standard, low-energy X-ray sources allow only to determine the average layer behaviour, and not the variation in mechanical properties within the SP-affected layer. Promisingly, the use of intense, hard (energy ≥50 keV) X-ray synchrotron sources and micro-focusing optics offers the opportunity to depth profile the local behaviour within the material under straining [25,26]. The aim of this work is therefore to determine the local elasto-plastic behaviour within the (sub)surface layer in 7050-T7451 aluminium alloy treated using two different shot peening intensities. This approach has not yet been explored to fully characterise the variation in local mechanical properties within SP-treated surfaces in aerospace Al-base alloys.

2. Materials and methods

2.1. Shot peening

Table 1 shows the chemical composition of the 7050-T7451 rolled plate used in this study. The as-received microstructure consisted of both fine grains (average size of ~6 μm, grains ranging from 3 to 25 μm) and coarser grains elongated along the rolling direction of the initial plate material (average size of ~110 μm, grains ranging from 25 to 185 μm) in the matrix, see Figs. S1 and S2. The microstructure also contained ~1 vol% of secondary phases, namely Al_7Cu_2Fe and Mg_2Si [27,28], with a size varying from 1 to 2 to 30 μm and located predominantly within coarse matrix grains. Dog-bone specimens were machined with their long axis along the rolling direction of the initial plate material, see Fig. 1. Shot peening was applied to one side of the gauge length of the specimens, using a NORBLAST S8014SHOT pneumatic machine and S110 steel shots of 300 μm diameter. Two separate batches of specimens were prepared using either Low-intensity (LSP) or High-intensity (HSP) Shot Peening conditions, see Table 2. Samples for microstructural analysis were cut out from a representative specimen in each batch, mechanically polished and finally etched using Keller's reagent. A Leica DMi8 microscope was used for optical examination of the microstructure in the SP-induced layer, whereas the surface roughness was characterised using an Alicona IFG4 optical profilometer. Complementarily, the mechanical properties induced by LSP and HSP were initially assessed by nanoindentation employing a Bruker/Hysitron TI 980 Select equipment. For this purpose, the samples used in the optical microscopy analysis, were re-ground and re-polished. The equipment stability and indentation repeatability were tested by doing 10 indents into a piece of fused silica with a theoretical hardness value of 9.25 GPa. The results of the calibration were within tolerance with an average error of 7 % (see Fig. S3). A Berkovich tip was used under displacement control, doing indentations up to a 200 nm depth with a spacing of 5 μm to avoid side effects. Up to 30 μm depth, the scan line was tilted with respect to the surface, to obtain nanoindentations with a spacing of 1 μm in the perpendicular direction to the shot peened surface. From 30 μm to 500 μm depth, the nanoindentations were done with a spacing of 5 μm. Data was processed applying the Oliver Pharr method [29].

2.2. In-situ diffraction under straining

In-situ synchrotron X-ray diffraction (SXRD) experiments of the shot peened specimens were sequentially done at room temperature using a 2 kN Deben micro-tensile rig installed at the high-energy I12 beamline of the UK Diamond Light Source, see Fig. 2a. A monochromatic X-ray beam with an energy of 80 keV ($\lambda = 0.1550$ Å) and a 100×100 μm^2 spot size illuminated the specimen. A tensile test was carried out in elongation steps of ~0.1 mm to specimen rupture. At each deformation step, the sample was kept at constant displacement, and three 1.0 mm horizontal line scans were done by translating the specimen with respect to the incident X-ray beam in steps of 0.1 mm, starting from the shot peened surface of the specimen gauge length, see Fig. 2b. At each specimen position, a 2-D diffraction pattern was collected in transmission geometry using a Thales Pixium RF4343 2-D area detector placed behind the specimen at a distance of ~630 mm. The experimental geometry was calibrated using a CeO_2 standard (NIST Standard Reference Material 674b) [31].

The recorded 2-D dataset was integrated using the DAWN software package [32] to obtain the longitudinal ($\varepsilon_{hkl,L}$) and transverse ($\varepsilon_{hkl,T}$) lattice strains, parallel and perpendicular to the loading direction respectively, see Fig. 2b. The resultant 1-D patterns were analysed using a single-peak fitting process to a pseudo-Voigt profile. The lattice strains at each specimen position and applied stress were then calculated according to:

$$\varepsilon_{hkl} = \frac{d_{hkl} - d^0_{hkl}}{d^0_{hkl}} \quad (1)$$

where d_{hkl} and d^0_{hkl} are the lattice plane spacing at a given loading increment and at zero deformation, respectively. The d^0_{hkl} value was determined by averaging the experimental d_{hkl} values at positions from 0.8 to 1 mm at zero applied stress, since shot peening did not induce significant residual stresses at depths greater than 0.5 mm.

3. Results

3.1. Shot peened surfaces

Fig. 3a & b shows the longitudinal-sectional view of the near surface microstructure and topography of the surface after the LSP and HSP

Table 1
Chemical composition (in wt.%) of the 7050-T7451 alloy used in this study.

Zn	Mg	Cu	Zr	Fe	Si	Ti	Cr	Mn	V	Other	Al
6.22	2.00	1.87	0.11	0.06	0.02	0.01	0.01	0.01	0.01	<0.01	Bal.

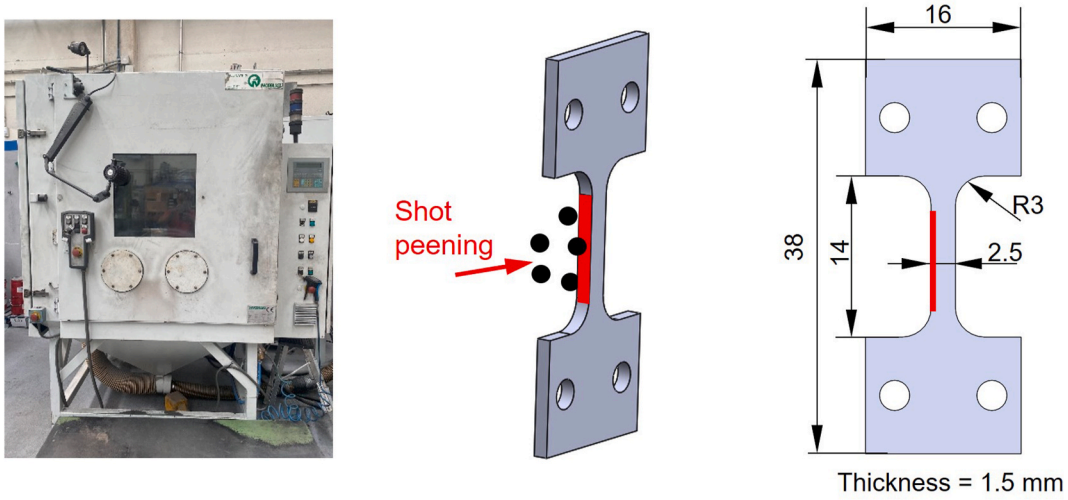

Fig. 1. Shot peening NORBLAST S8014SHOT pneumatic machine, geometry of the dog-bone specimen and identification of the area treated by shot peening.

Table 2
Parameters used during the shot peening treatment of 7050-T7451 alloy prior to the in-situ synchrotron experiment, using either Low-Intensity (LSP) or High-Intensity (HSP) Shot Peening. Shot peened surfaces were inspected with a magnifying glass and coverage was determined following the SAE J2277 standard [30], exposing the specimens to shots >1.25 times the exposure time required to obtain 98 % coverage.

Parameter	LSP	HSP
Balls/Shots	S110 (58–60 HRC)	S110 (58–60 HRC)
Flow (kg/min)	9.93	6.97
Pressure (bar)	1.5	4
Almen Intensity (A)	3.4	10.9
Coverage (%)	>125	>125

treatments, and Fig. 3c displays the nanohardness profile of both surface conditions. LSP did not produce observable alterations in grain structure near the surface, only an irregular surface with localised bent grains up to a ~5 μm depth due to the deformation caused by the shots. In contrast, HSP led to a visible surface layer of ~20–30 μm in thickness with severe plastic deformation (SPD). The surface irregularities induced by the impacts are also visible on the surface treated by HSP, where some material from protruding peaks also became folded due to the repetitive impacts. Consequently, the LSP and HSP treatments generated clear differences in surface roughness, i.e. HSP produced an arithmetical mean height of *Sa* ~13 μm and a maximum peak height of *Sp* ~51 μm, whereas LSP led to *Sa* ~2 μm and *Sp* ~16 μm. Although both shot peening intensities produce different surface characteristics, the hardness value was not modified with respect to the bulk material (~2.5 GPa).

3.2. Bulk mechanical behaviour

Fig. 4a displays the macroscopic behaviour of an unpeened (UP) specimens as reference, and the specimens treated by LSP and HSP. In all conditions, the material showed similar elastic and flow stress behaviour. The experimental values of the yield stress (σ_y) were 430 MPa (UP), 450 MPa (LSP) and 435 MPa (HSP), whereas the rupture stress (σ_u) was 490 MPa (UP), 515 MPa (LSP) and 480 MPa (HSP), respectively. We also measured the mechanical behaviour of the as-received material, prior to shot peening treatment, using standard macroscopic specimens with 6 mm diameter and 36 mm gauge length, and obtained the values of elastic modulus E = 70.9 GPa, σ_y = 480 MPa and σ_u = 575 MPa. The geometry of the standard specimens and an example of the measured stress-strain curve can be found in Fig. S4. These differences between as-received and SP-treated materials can be due to differences in specimen's geometry [33], rather than an effect of the thin SP-induced layers on the macroscopic behaviour of the material since the area affected by SP is less than the 15 % of the cross-section. Despite these slight differences in the mechanical properties, the specimens used in the in-situ tests represented the bulk behaviour of the polycrystal up to the rupture stress, because they satisfied the design criteria of miniaturised flat specimens [33]: i) thickness (t) to grain size (d) ratio $t/d = 13.6 > 10$ and ii) width (w) to thickness ratio $w/t = 1.7 < 5$.

Fig. 4b, 4c, 4d & 4e show the evolution of the longitudinal lattice strain ($\varepsilon_{hkl,L}$) with respect to the applied strain and the Full-Width-at-Half-Maximum (FWHM) for hkl = 220, 311 and 420, of both LSP-treated and HSP-treated specimens, measured at a distance of x = 1 mm from the SP-affected surface. The 111, 200, and 331 reflections showed similar behaviour to those included in Fig. 4b–e. There is a linear behaviour up to ~0.25 applied strain. Upon reaching the yield stress, the measured longitudinal lattice strain relaxes somewhat, and then continues to increase slightly with further increase in applied strain. The values of the E_{hkl} elastic modulus can be calculated using:

$$E_{hkl} = \frac{\sigma}{\varepsilon_{hkl,L}} \tag{2}$$

where σ is the applied stress, see Table 3. Moreover, the values of FWHM remained constant up to ~0.25 applied strain, and thereafter increased with the applied strain, as evidence of the occurrence of plastic deformation in the bulk microstructure.

3.3. Behaviour of SP-induced surface layers

Figs. 5 and 6 show the evolution of the longitudinal lattice strain profiles ($\varepsilon_{hkl,L}$) in the LSP- and HSP-treated specimens with applied stress, respectively. The simultaneous changes in transverse lattice strains ($\varepsilon_{hkl,T}$) with applied stress are provided in Figs. S5 and S6. Both shot peening conditions induced compressive residual lattice strains in the longitudinal direction, i.e. perpendicular to the shot peening direction. LSP generated a ~0.2 mm thick compressive layer and a maximum compressive lattice strain of ~3000 με was reached at the surface, ~60 % of the tensile lattice strain reached when yielding occurs in the bulk material (~5000 με, see Fig. 4b and c). The thickness of the compressive layer increased up to ~0.4 mm when applying HSP conditions, as consequence of the higher plastic deformation induced by the shots impacting at higher energy. HSP produced lower lattice strains at the surface than LSP, but higher maximum compressive lattice strains within the SP-induced layer. In fact, HSP induced the maximum compressive

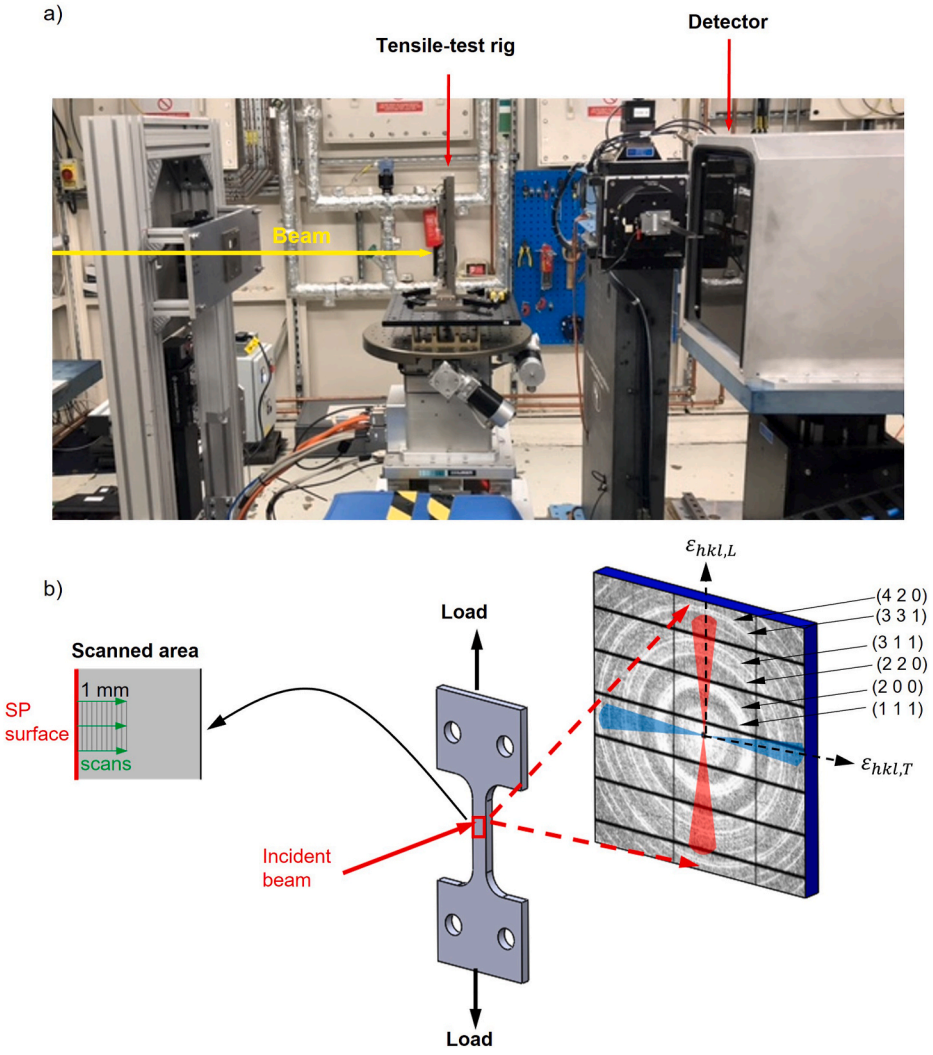

Fig. 2. (a) Synchrotron beamline set-up and (b) schematic of the experimental geometry used for the in-situ synchrotron X-ray diffraction experiments of the dog-boned specimens after having undergone a shot peening treatment on their gauge length.

peak at ~0.1 mm depth, ranging values from ~3000 to 4500 με, i.e. ~60–90 % of the lattice strain at the yield stress of the bulk material, depending on the analysed *hkl*-reflection. Complementarily, shot peening induced tensile residual lattice strains in the transverse direction prior to the SXRD experiment.

Longitudinal lattice strain profiles shifted from compressive to tensile for both types of specimens, when applying tensile loads below the yield stress of the bulk material. Above the yield stress, the bulk material started yielding first, as evidenced by a homogenous lattice strain magnitude at higher depths. Lower lattice strains were observed near the surface, since they were initially compressive. However, at higher applied stresses the entire cross section of the specimen yielded, and a uniform lattice strain level was reached throughout the specimen. Complementarily, compressive lattice strains were measured in the transverse direction upon materials loading, attaining a uniform compressive lattice strain across the specimen. This magnitude of lattice strain was lower than in the longitudinal direction, in accordance with the Poisson's ratio of the as-received material ($\nu \sim 0.3$).

4. Discussion

LSP and HSP treatments induced a 0.2 mm- and 0.4 mm-thick compressive layer in the longitudinal direction of the specimen, respectively. Due to successive high-energy impacts during the SP treatment, the grains near the surface are strained parallel to the surface, whereas the bulk material remains undeformed. To reach balance, compressive residual stresses are generated near the surface in the longitudinal direction of the specimen. In contrast, near-surface grains are compressed perpendicular to the surface, whereas the bulk material are undeformed. Consequently, tensile residual stresses are generated perpendicular to the surface for balance.

The observed effect of SP on the measured values of the quasi-static macroscopic mechanical properties for the tested conditions is not meaningful, as also reported by [34] in alloy 7075-T7351. LSP shows a slightly higher yield stress (15 MPa, 3.5 %) and ultimate tensile strength (35 MPa, 7 %) than the tested HSP. As described above, LSP only affected a thickness of 0.2 mm (8 % of the cross-section) and HSP impacted on 0.4 mm (16 % of the cross-section), and therefore the quasi-static (overall) behaviour of the specimen is dominated by the bulk performance of the material. Furthermore, the stress-strain curve of both SP-treated specimens follows the mechanical behaviour of the 'unpeened' or virgin condition (Fig. 4a). The slight differences observed between the LSP and HSP conditions are associated with the uncertainty of the measurement or small variations in the as-received material within the same batch. As it can be seen in Figs. 5 and 6, the bulk material of the specimen treated by LSP reached slightly higher lattice strains than the HSP specimen.

For discussion, Fig. 7a–b shows the evolution with applied strain of

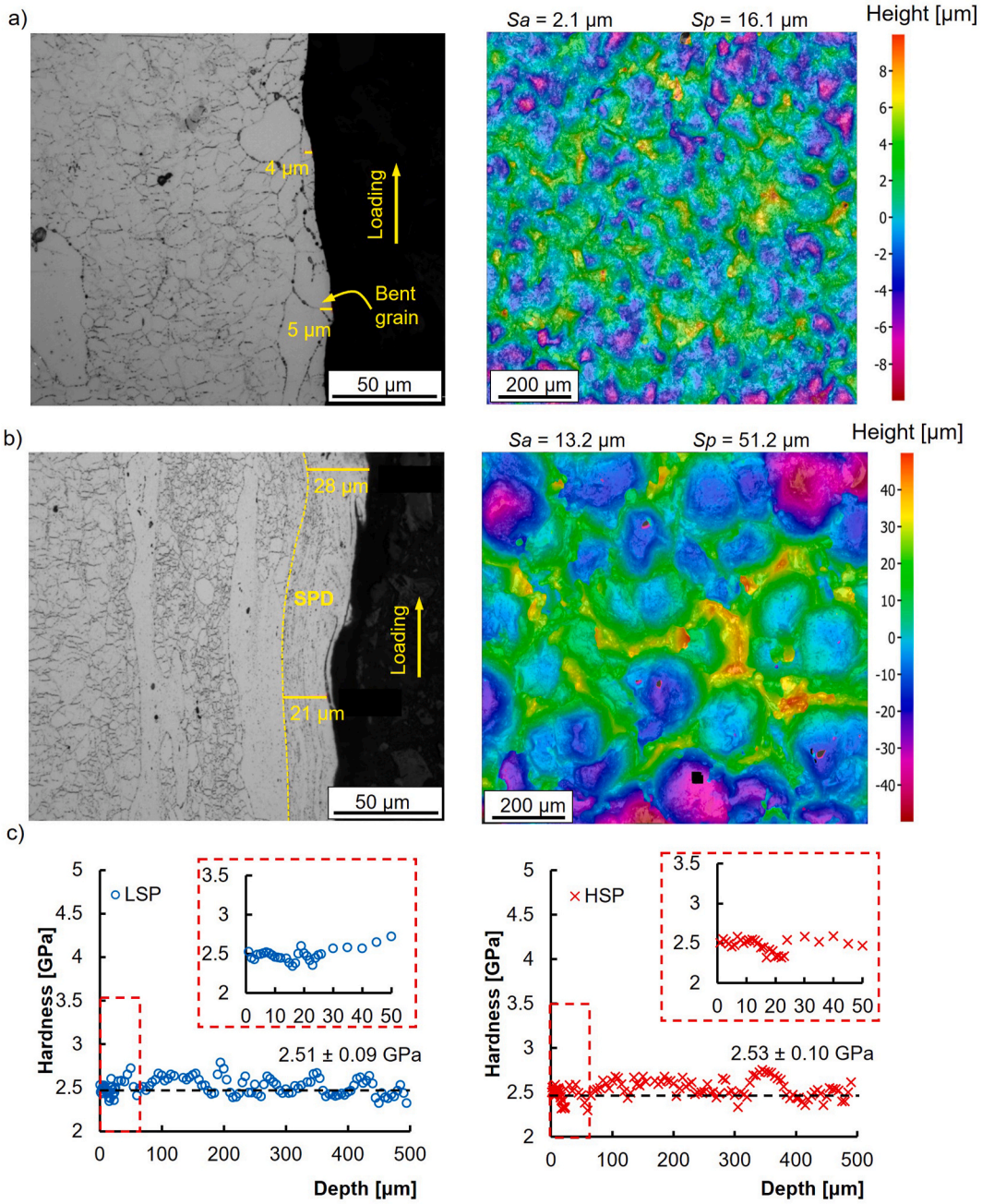

Fig. 3. The longitudinal-sectional view of the near surface microstructure (left) and surface view of the topography after the SP-treatment (right) of (a) the Low-intensity (LSP) and (b) High-intensity (HSP) shot peened specimen. Low-intensity shot peening only induced an irregular surface with localised bent grains up to ~5 µm in depth, whereas high-intensity shot peening led to a ~20–30 µm thick surface layer with severe plastic deformation (SPD). (c) Nanohardness profiles of both shot peened conditions.

the longitudinal 220-lattice strain at $x = 0.1$ and 0.3 mm from the SP-treated surface, together with the bulk material behaviour, based on the experimental data already presented in Figs. 5 and 6. The surface behaviour pre-yielding is affected by the shot peening treatment. The lattice strains at $x = 0.1$ mm did not increase linearly when elastically loading the specimen treated by LSP, whereas the layer at $x = 0.3$ mm and bulk material presented a similar, linear behaviour. In contrast, the lattice strains at both $x = 0.1$ and 0.3 mm in the HSP-treated specimen did not show a linear behaviour. Despite these differences, the local yield stress of the surface treated by LSP and HSP was not increased with respect to the yielding detected in the bulk material. This observation agrees with the nanohardness measurements (see Fig. 3c), which also did not show variations in hardness from the surface to the bulk. In this respect, 7050-T7451 alloy was reported to present only a slight strain rate sensitivity at room temperature [35,36], which was ascribed to the hindrance of local precipitates to dislocation motion [35]. Therefore, the local yield stress of the (near-)surface material was not modified, despite having been deformed at relatively high strain-rates during the SP treatment.

Furthermore, the evolution with applied stress of the 220-FWHM at $x = 0.1$ and 0.3 mm from the SP-treated surface, together with the bulk material behaviour, are displayed in Fig. 7c–d for the LSP- and HSP-treated specimens, respectively. Prior to the in-situ SXRD experiment, the FWHM at $x = 0.1$ mm was ~20 % (LSP) and ~40 % (HSP) higher than in the bulk material, evidencing the local plastic deformation induced near-surface in the material by the SP process. Moreover, the

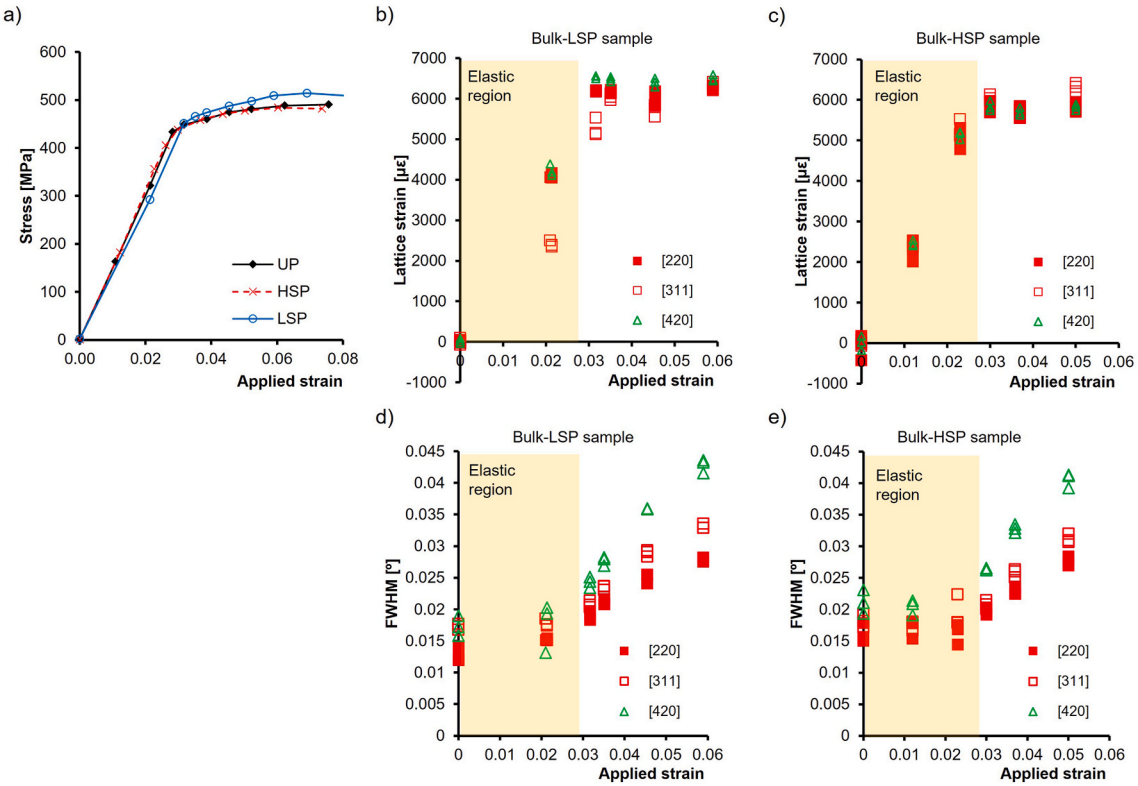

Fig. 4. (a) Macroscopic stress-strain curve of the 'unpeened' (virgin) specimen (UP) and specimens treated by High-intensity (HSP) and Low-intensity (LSP) Shot Peening (b) longitudinal lattice strain vs. applied strain and in the bulk structure (i.e. $x = 1$ mm from the peened surface), of the LSP-treated specimen and (c) of HSP-treated specimen, (d) FWHM vs. applied strain in the bulk structure of the LSP-treated specimen and (e) of the HSP-treated specimen.

Table 3
hkl-dependent elastic modulus corresponding to the specimens treated by Low-intensity (LSP) or High-intensity Shot Peening (HSP).

Plane	HSP E_{hkl} [MPa]	LSP E_{hkl} [MPa]	Average E_{hkl} [MPa]
110	74.2	80.2	77.2
200	76.7	71.2	74.0
220	66.9	70.6	68.8
311	65.9	67.1	66.5
331	70.4	70.6	70.5
420	67.1	75	71.0

FWHM was ~20 % higher than the bulk material at $x = 0.3$ mm in the surface treated by HSP, whereas an increase in FWHM was not observed at the same position in the HSP-treated specimen. These results confirm that HSP induced a higher plastic deformation and a thicker affected layer than LSP. The value of the FWHM measured at $x = 0.1$ mm significantly increased for both LSP and HSP conditions, when increasing the applied stress prior to the material's yielding. This observation agrees with the non-linearity of the lattice strains previously discussed. At the yield stress of the material, the FWHM values of both SP-treated surfaces slightly decreased, see points outlined with a dashed line in Fig. 7c–d. This could be due to a local re-organization of the lattice defects withing the SP-induced layer. Further increase of the applied strain post-yield stress of the bulk material induces plastic deformation throughout the entire cross section of both specimens. Consequently, the FWHM increased almost linearly post-yielding in both SP-induced layers, while maintaining higher values as compared to the bulk material, due to the SP-induced plasticity prior to the in-situ SXRD experiment.

As described in the introduction existing models do not predict accurately the relaxation of residual stresses and fatigue crack propagation during mechanical fatigue loading in Al-based alloys. Recent fatigue models incorporate the relaxation of residual stresses and the evolution of the cold work (plastic deformation) to predict crack initiation and propagation in shot peened specimens [19,37]. Although we tested the quasi-static mechanical properties of the shot peening affected layer in 7050-T7451 aluminium alloy, the results could be useful as input to develop and potentially validate those models. In fact, the main relaxation of peening induced compressive residual stresses occurs during the first cycle [23,24,38] and they further relax during cyclic loading. Theoretically, the relaxation of compressive residual stresses occurs if the core material reaches the yield stress before the surface layer [39]. This work has found that the yield stress of the SP-affected surface (for the selected SP parameters) is similar to the bulk material, and therefore compressive residual stresses should in principle not relax significantly under high cycle fatigue conditions (applied stresses significantly lower than the yield stress). However, our study has confirmed that the severely deformed layer does not behave linearly during tensile loading in the elastic region of the material, and that accumulates further plastic deformation beyond yielding. This behaviour could be used to model the evolution of cold work based on FWHM [19,37]. The plastic strain distribution through the thickness of as-SP materials can be modelled using eigenstrain distributions and validated normally using destructive X-ray diffractometry [40], and this approach could potentially be extended for fatigue lifetime prediction [41].

The methodology proposed in this work has been satisfactorily applied to characterise non-destructively the initial strain distribution in the as-SP condition, but also the depth-resolved local mechanical behaviour of shot peened aluminium specimens under quasi-static loading, both prior and post-yielding of the material. The proposed method could also be in the future be extended to characterise the cyclic mechanical response of shot peened surfaces and bulk material, which could undoubtedly help to develop more sophisticated fatigue life prediction models.

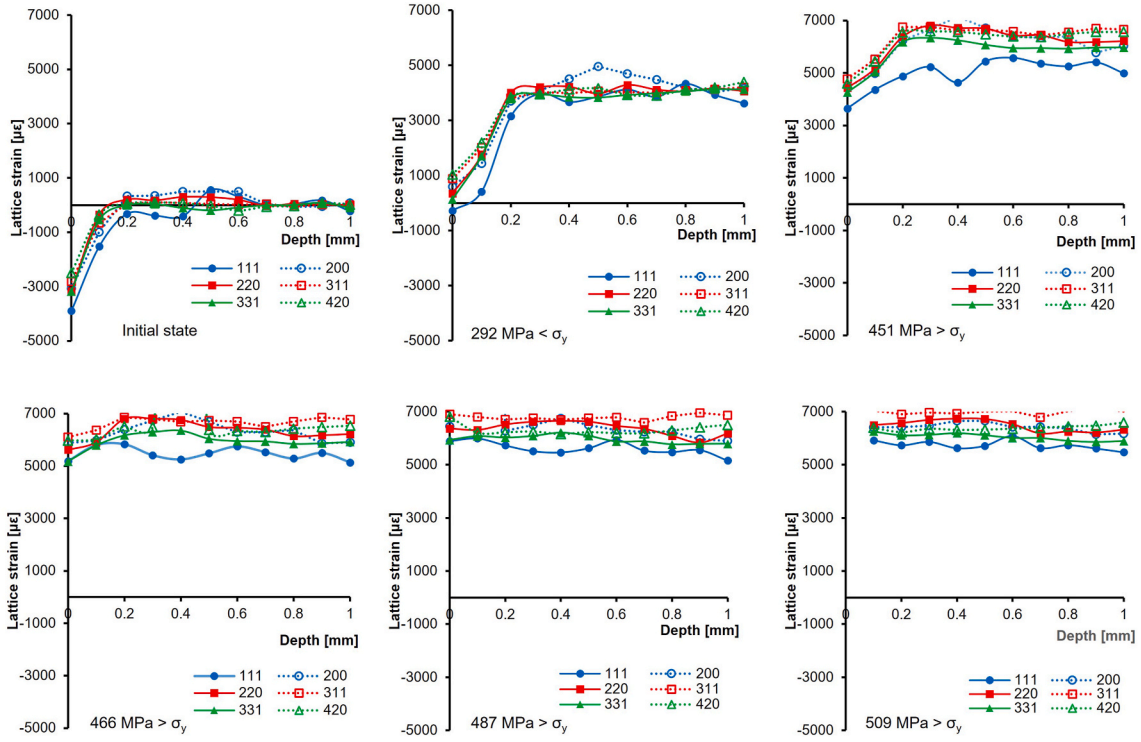

Fig. 5. Longitudinal lattice strain profiles of the specimen treated by Low-intensity Shot Peening (LSP) at selected applied stress levels. σ_y denotes the yield stress of the material.

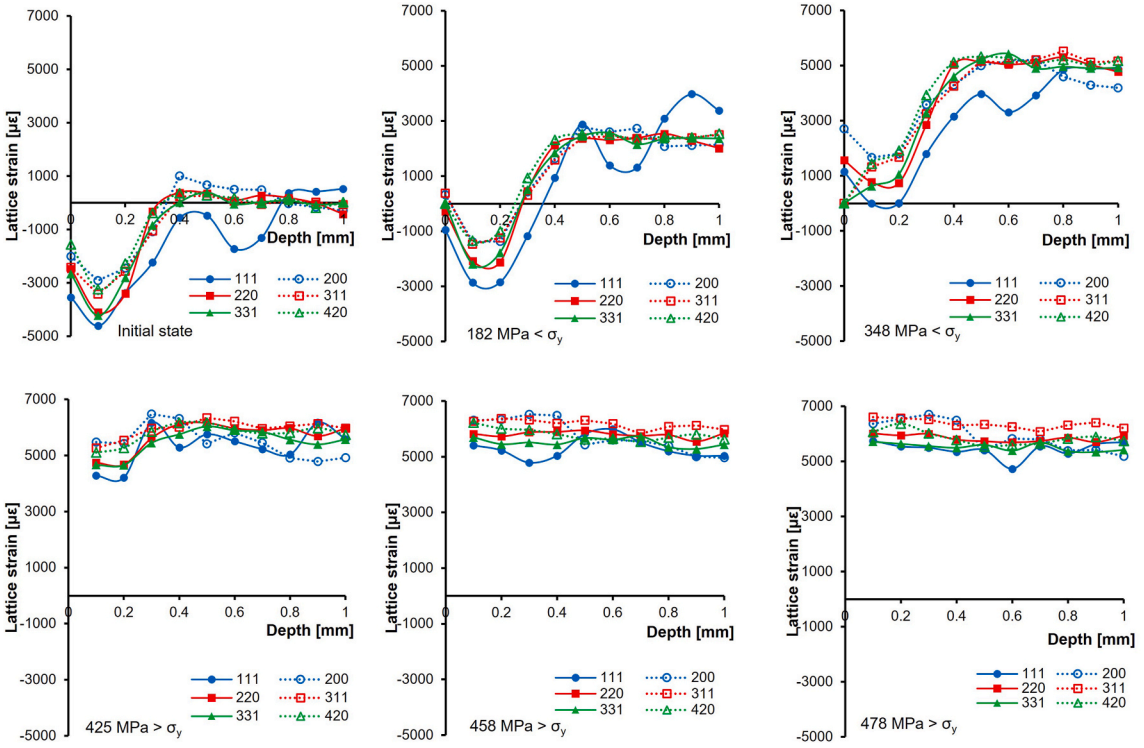

Fig. 6. Longitudinal lattice strain profiles of the specimen treated by High-intensity Shot Peening (HSP) at selected applied stress levels. σ_y denotes the yield stress of the material.

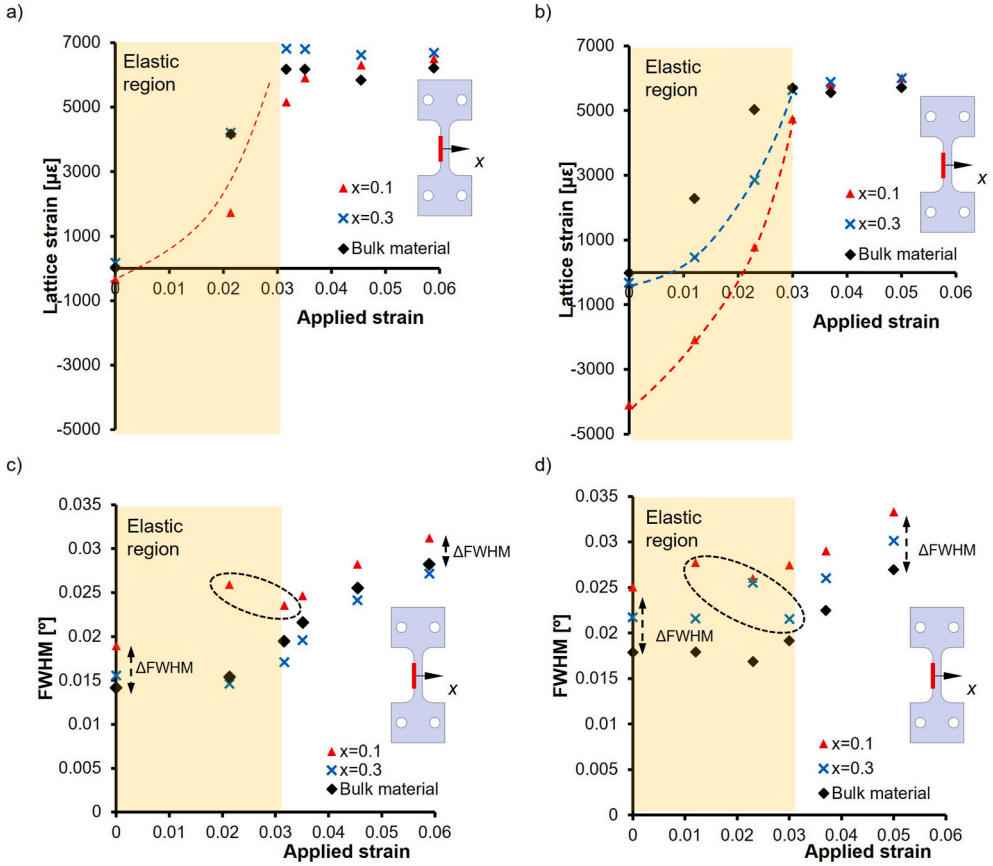

Fig. 7. Longitudinal 220-lattice strain and FWHM vs. applied stress near the surface (x = 0.1 and 0.3 mm) and in the bulk microstructure, in the specimen treated with (a, c) Low- and (b, d) High-intensity Shot Peening.

5. Conclusions

This work probed the mechanical properties of two types of shot peening affected layers in 7050-T7451 aluminium alloy at room temperature, by combining in-situ tensile testing and synchrotron X-ray diffraction measurements in transmission geometry. The main conclusions are.

- Low-intensity shot peening did not induce visible alterations in grain structure near the surface of the material, but high-intensity shot peening generated a clear plastic deformation layer with a thickness of ~20–30 μm.
- High-intensity shot peening led to rougher surfaces (Sa ~13 μm) than low-intensity shot peening (Sa ~2 μm).
- Both peening conditions induced compressive lattice strains in the longitudinal direction (i.e. perpendicular to the shot peening direction), and tensile in the transverse direction with respect to the applied load. High-intensity shot peening generated a two times thicker compressed layer and higher compressive lattice strains than low-intensity shot peening.
- The yield stress of the (sub)surface layer affected by shot peening did not vary with respect to the bulk material despite having applied two different shot peening intensities. Nevertheless, the elastic behaviour of the shot peening affected layer differs from the bulk material, since it does not show a linear behaviour (lattice strain vs applied strain) upon loading the specimen.
- Post-yielding of the material, the presence of SP-affected layers is only evidenced by the higher value of the FWHM than in the bulk material, primarily due to the prior SP-induced plasticity, since the lattice strains become uniform throughout the cross section of the material. Those highly deformed layers also accumulate some additional plastic deformation when applying elastic loads.

CRediT authorship contribution statement

A. Madariaga: Writing – original draft, Methodology, Investigation, Formal analysis, Conceptualization. **E. Vázquez:** Writing – review & editing, Resources, Investigation. **D. Foster:** Writing – review & editing, Investigation. **E. Jimenez-Melero:** Writing – review & editing, Supervision, Resources, Methodology, Investigation, Conceptualization.

Declaration of competing interest

The authors declare that they have no known competing financial interests or personal relationships that could have appeared to influence the work reported in this paper.

Data availability

Data will be made available on request.

Acknowledgments

This work was supported by EPSRC through the LOFAMO project (EP/X023281/1). We also acknowledge the UK Diamond Light Source for the granted time on the I12 beam line under the proposal MG24327-1. The authors acknowledge the Nanomechanical Characterisation Laboratory in the Department of Materials of The University of Manchester.

Appendix A. Supplementary data

Supplementary data to this article can be found online at https://doi.org/10.1016/j.msea.2024.146817.

References

[1] I.N. Fridlyander, Aluminum alloys in aircraft in the periods of 1970–2000 and 2001–2015, Met. Sci. Heat Treat. 43 (1) (2001) 6–10, https://doi.org/10.1023/A:1010453702596.

[2] I. Perez, A. Madariaga, M. Cuesta, A. Garay, P.J. Arrazola, J.J. Ruiz, F.J. Rubio, R. Sanchez, Effect of cutting speed on the surface integrity of face milled 7050-T7451 aluminium workpieces, Procedia CIRP 71 (2018) 460–465, https://doi.org/10.1016/j.procir.2018.05.034.

[3] L.G. Li, S.Q. Wang, Distortion caused by residual stresses in machining aeronautical aluminum alloy parts: recent advances, Int. J. Adv. Manuf. Technol. 89 (1) (2017) 997–1012, https://doi.org/10.1007/s00170-016-9066-6.

[4] C.F. Yao, X. Dou, D. Wu, Z. Zhou, J. Zhang, Surface integrity and fatigue analysis of shot-peening for 7055 aluminum alloy under different high-speed milling conditions, Adv. Mech. Eng. 8 (10) (2016) 1–10, https://doi.org/10.1177/1687814016674628.

[5] G.H. Majzoobi, K. Azadikhah, J. Nemati, The effects of deep rolling and shot peening on fretting fatigue resistance of Aluminum-7075-T6, Mater. Sci. Eng., A 516 (1–2) (2009) 235–247, https://doi.org/10.1016/j.msea.2009.03.020.

[6] X. Tao, Y. Gao, Effects of wet shot peening on microstructures and mechanical properties of a 2060-T8 aluminum-lithium alloy, Mater. Sci. Eng., A 832 (2022) 142436, https://doi.org/10.1016/j.msea.2021.142436.

[7] Y.K. Gao, Improvement of fatigue property in 7050–T7451 aluminum alloy by laser peening and shot peening, Mater. Sci. Eng., A 528 (10–11) (2011) 3823–3828, https://doi.org/10.1016/j.msea.2011.01.077.

[8] T. Kostilnik, Shot peening, in: ASM Handbook, Surface Engineering, vol. 5, ASM International, USA, 1994, https://doi.org/10.31399/asm.hb.v05.a0001235.

[9] M.R. Isa, O.S. Zaroog, P. Raj, S.N. Sulaiman, I. Abu Shah, I.N. Ismail, et al., Numerical analysis of shot peening parameters for fatigue life improvement, AIP Conf. Proc. 2030 (2018) 020217, https://doi.org/10.1063/1.5066858.

[10] Y. Mutoh, G.H. Fair, B. Noble, R.B. Waterhouse, The effect of residual stresses induced by shot-peening on fatigue crack propagation in two high strength aluminium alloys, Fatig. Fract. Eng. Mater. Struct. 10 (4) (1987) 261–272, https://doi.org/10.1111/j.1460-2695.1987.tb00205.x.

[11] M. Benedetti, V. Fontanari, P. Scardi, C.A. Ricardo, M. Bandini, Reverse bending fatigue of shot peened 7075-T651 aluminium alloy: the role of residual stress relaxation, Int. J. Fatig. 31 (8–9) (2009) 1225–1236, https://doi.org/10.1016/j.ijfatigue.2008.11.017.

[12] U. Zupanc, J. Grum, Surface integrity of shot peened aluminium alloy 7075-T651, J. Mech. Eng. 57 (2011) 379–384, https://doi.org/10.5545/sv-jme.2010.142.

[13] C. Yao, L. Ma, Y. Du, J. Ren, D. Zhang, Surface integrity and fatigue behavior in shot-peening for high-speed milled 7055 aluminum alloy, Proc IMechE Part B: J. Eng. Manuf. 231 (2) (2017) 243–256, https://doi.org/10.1177/0954405415573704.

[14] H. Luong, M.R. Hill, The effects of laser peening and shot peening on high cycle fatigue in 7050-T7451 aluminum alloy, Mater. Sci. Eng., A 527 (3) (2010) 699–707, https://doi.org/10.1016/j.msea.2009.08.045.

[15] M. Benedetti, V. Fontanari, M. Bandini, E. Savio, High-and very high-cycle plain fatigue resistance of shot peened high-strength aluminum alloys: the role of surface morphology, Int. J. Fatig. 70 (2015) 451–462, https://doi.org/10.1016/j.ijfatigue.2014.07.002.

[16] A. Becker, The Effect of Laser Shock Peening and Shot Peening on the Fatigue Performance of Aluminium Alloy 7075, University of Cape Town, 2017. PhD Thesis.

[17] Y.K. Gao, X.R. Wu, Experimental investigation and fatigue life prediction for 7475-T7351 aluminum alloy with and without shot peening-induced residual stresses, Acta Mater. 59 (9) (2011) 3737–3747, https://doi.org/10.1016/j.actamat.2011.03.013.

[18] l. Wagner, Mechanical surface treatments on titanium, aluminum and magnesium alloys, Mater. Sci. Eng., A 263 (1999) 210–216, https://doi.org/10.1016/S0921-5093(98)01168-X.

[19] C. Bianchetti, D. Delbergue, P. Bocher, M. Lévesque, M. Brochu, Analytical fatigue life prediction of shot peened AA 7050-T7451, Int. J. Fatig. 118 (2019) 271–281, https://doi.org/10.1016/j.ijfatigue.2018.07.007.

[20] J.P. Nobre, A.C. Batista, L. Coelho, A.M. Dias, Two experimental methods to determining stress–strain behavior of work-hardened surface layers of metallic components, J. Mater. Process. Technol. 210 (2010) 2285–2291, https://doi.org/10.1016/j.jmatprotec.2010.08.019.

[21] L. Coelho, A.C. Batista, J.P. Nobre, M.J. Marques, Evaluation of stress-strain behavior of surface treated steels by X-ray diffraction, Cent. Eur. J. Eng. 2 (1) (2012) 91–95, https://doi.org/10.2478/s13531-011-0051-4.

[22] K. Zhan, C.H. Jiang, V. Ji, Surface mechanical properties of S30432 austenitic steel after shot peening, Appl. Surf. Sci. 258 (24) (2012) 9559–9563, https://doi.org/10.1016/j.apsusc.2012.05.122.

[23] L. Xie, Y. Wen, K. Zhan, L. Wang, C. Jiang, V. Ji, Characterization on surface mechanical properties of Ti–6Al–4V after shot peening, J. Alloys Compd. 666 (2016) 65–70, https://doi.org/10.1016/j.jallcom.2016.01.119.

[24] M. Chen, S. Xing, H. Liu, C. Jiang, K. Zhan, V. Ji, Determination of surface mechanical property and residual stress stability for shot-peened SAF2507 duplex stainless steel by in situ X-ray diffraction stress analysis, J. Mater. Res. Technol. 9 (4) (2020) 7644–7654, https://doi.org/10.1016/j.jmrt.2020.05.028.

[25] D.M. Collins, M. Mostafavi, R.I. Todd, T. Connolly, A.J. Wilkinson, A synchrotron X-ray diffraction study of in situ biaxial deformation, Acta Mater. 90 (2015) 46–58, https://doi.org/10.1016/j.actamat.2015.02.009.

[26] D. Foster, M. Paladugu, J. Hughes, M. Kapousidou, C. Barcellini, D. Daisenberger, E. Jimenez-Melero, Comparative micromechanics assessment of high-carbon martensite/bainite bearing steel microstructures using in-situ synchrotron X-ray diffraction, Materialia 14 (2020) 100948, https://doi.org/10.1016/j.mtla.2020.100948.

[27] Z. Zhong, X. Ai, Z. Liu Z., J. Liu, Q. Xu, Surface morphology and microcrack formation for 7050-T7451 aluminum alloy in high speed milling, Int. J. Adv. Manuf. Technol. 78 (1–4) (2015) 281–296, https://doi.org/10.1007/s00170-014-6605-x.

[28] Y. Liu, C. Deng, B. Gong, B.Y. Bai, Effects of heterogeneity and coarse secondary phases on mechanical properties of 7050-T7451 aluminum alloy friction stir welding joint, Mater. Sci. Eng., A 764 (2019) 138223, https://doi.org/10.1016/j.msea.2019.138223.

[29] W.C. Oliver, G.M. Pharr, Measurement of hardness and elastic modulus by instrumented indentation: advances in understanding and refinements to methodology, J. Mater. Res. 19 (1) (2004) 3–20, https://doi.org/10.1557/jmr.2004.19.1.3.

[30] SAE International, "Shot Peening Coverage Determination," SAE Stand, J2277, 2023.

[31] M. Hart, M. Drakopoulos, C. Reinhard, T. Connolly, Complete elliptical ring geometry provides energy and instrument calibration for synchrotron-based two-dimensional X-ray diffraction, J. Appl. Crystallogr. 46 (5) (2013) 1249–1260, https://doi.org/10.1107/S0021889813022437.

[32] J. Filik, A.W. Ashton, P.C.Y. Chang, P.A. Chater, S.J. Day, M. Drakopoulos, M. W. Gerring, M.L. Hart, O.V. Magdysyuk, S. Michalik, A. Smith, Processing two-dimensional X-ray diffraction and small-angle scattering data in DAWN 2, J. Appl. Crystallogr. 50 (3) (2017) 959–966, https://doi.org/10.1107/S1600576717004708.

[33] P. Zheng, R. Chen, H. Liu, J. Chen, Z. Zhang, X. Liu, Y. Shen, Y. On the standards and practices for miniaturized tensile test–A review, Fusion Eng. Des. 161 (2020) 112006 1–11200611, https://doi.org/10.1016/j.fusengdes.2020.112006.

[34] O. Hatamleh, The effects of laser peening and shot peening on mechanical properties in friction stir welded 7075-T7351 aluminum, J. Mater. Eng. Perform. 17 (2008) 688–694, https://doi.org/10.1007/s11665-007-9163-7.

[35] F. Jiang, J. Li, J. Sun, S. Zhang, Z. Wang, L. Yan, Al7050-T7451 turning simulation based on the modified power-law material model, Int. J. Adv. Manuf. Technol. 48 (2010) 871–880, https://doi.org/10.1007/s00170-009-2328-9.

[36] G. Chen, C. Ren, Z. Ke, J. Li, X. Yang, Modeling of flow behavior for 7050-T7451 aluminum alloy considering microstructural evolution over a wide range of strain rates, Mech. Mater. 95 (2016) 146–157, https://doi.org/10.1016/j.mechmat.2016.01.006.

[37] T. Klotz, H.Y. Miao, C. Bianchetti, M. Lévesque, M. Brochu, Analytical fatigue life prediction of shot peened Inconel 718, Int. J. Fatig. 113 (2018) 204–221, https://doi.org/10.1016/j.ijfatigue.2018.04.011.

[38] V. Schulze, Modern Mechanical Surface Treatment: States, Stability, Effect, John Wiley & Sons, Weinheim, 2006.

[39] A. Madariaga, J.A. Esnaola, P.J. Arrazola, J. Ruiz-Hervias, P. Muñoz, P.K. Ostolaza, Stability of machining induced residual stresses in Inconel 718 under quasi-static loading at room temperature, Mater. Sci. Eng., A 620 (2015) 129–139, https://doi.org/10.1016/j.msea.2014.09.118.

[40] A.M. Korsunsky, On the modelling of residual stresses due to surface peening using eigenstrain distributions, J. Strain Anal. 40 (8) (2005) 817–824, https://doi.org/10.1243/030932405X30984.

[41] D. Petukhov, I. Keller, Exact reconstruction formulas for plastic strain distribution in the surface-treated plate and their applications, Acta Mech. 231 (2020) 1849–1866, https://doi.org/10.1007/s00707-020-02625-7.